

Electronic supplementary information

S1 Estimates of the equilibrium O₂ and CO₂ partial pressures

The equilibrium O₂ and CO₂ partial pressures, p_{O_2} and p_{CO_2} , respectively, have been estimated for the temperature range of 1000 -2000°C by solving the equation set

$$K_2(T) = p_{Mg} p_{O_2}^{0.5} \quad (S1)$$

$$K_4(T) = \frac{p_{Mg} p_{CO_2}}{p_{CO}} \quad (S2)$$

using the equilibrium constants $K_i(T)$ that were extracted from the HSC database.¹ Equation S2 was solved assuming that $p_{CO} = p_{Mg}$ as imposed by the stoichiometry of the overall reaction. The results for p_{Mg} of 1, 10 and 100 Pa are plotted in Figure S1, demonstrating that the equilibrium O₂ and CO₂ partial pressures are rather low. For example, at 1400°C the equilibrium values for p_{O_2} range from 10⁻¹⁴ to 10⁻¹⁰ Pa while the equilibrium p_{CO_2} is in the order of 10⁻³ Pa. Any increase in p_{O_2} and p_{CO_2} above these values is thus expected to shift the equilibria of reactions 2 and 4 towards the reactant side, thereby suppressing the Mg production.

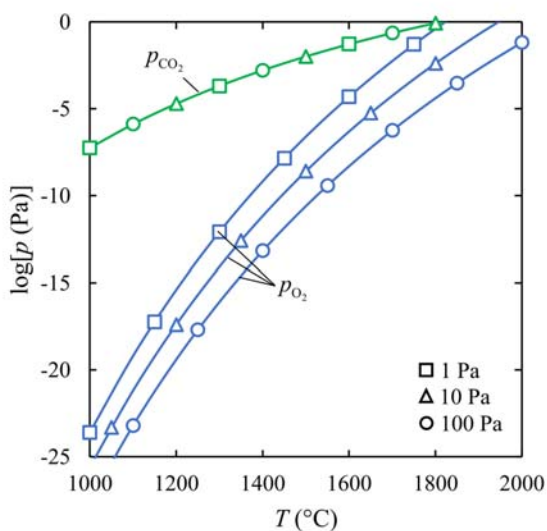


Figure S1. Equilibrium p_{O_2} and p_{CO_2} based on reactions 2 and 4 for $p_{Mg} = p_{CO} = 1, 10, \text{ and } 100 \text{ Pa}$.
Note: according to equation S2, the assumption $p_{Mg} = p_{CO}$ makes p_{CO_2} function of temperature only.

S2 Experimental program

Table S1. Experimental program comprising three phases with the tests under (1) O₂-Ar sweep, (2) CO₂-Ar sweep, and (3) CO-Ar sweep and Ar alone.

Phase	1 Detection of the onset of CTR and assessment of the C removal under O ₂ -Ar sweep	2 Detection of the onset of CTR and assessment of the C removal under CO ₂ -Ar sweep	3 Reference CTR experiments
Objectives	For a selected set of $N_{\text{ClO}_2}^0$, N_{MgO}^0 , and the flow rate and the composition of the O ₂ -Ar sweep determine <ol style="list-style-type: none"> $\tau_1 _{\text{O}_2}$, $\tilde{N}_{\text{ClO}_2}(\tau_1)$ and $\tilde{N}_{\text{ClO}_2}(\tau_f)$, $\tilde{p}'_{\text{CO} _{\text{O}_2}}$, and the extent of the CTR. 	<ol style="list-style-type: none"> Establish a combination of the (i) the initial amount of C ($N_{\text{ClCO}_2}^0$) and (ii) CO₂-Ar sweep gas mixture flow rate and composition that for the selected temperature program defined in phase I leads to $\tilde{N}_{\text{ClCO}_2}(\tau_1) \approx \tilde{N}_{\text{ClO}_2}(\tau_1)$ and $\tilde{N}_{\text{ClCO}_2}(\tau_f) \approx \tilde{N}_{\text{ClO}_2}(\tau_f)$ (see Figure 3). Quantify the CO partial pressure ($\tilde{p}'_{\text{CO} _{\text{CO}_2}}$) for the previously established combination of reaction conditions. Determine the extent of the CTR. 	<ol style="list-style-type: none"> Determine the referent range of the CTR extents in the absence of any oxidant in the sweep to account for the effects of <ol style="list-style-type: none"> the consumption of C by the oxidants observed at step 12 of phase 1, and the difference in the partial pressures of CO observed in step 12 of phase 1 and step 14 of phase 2.
Materials	MgO-C blend and C in the absence of MgO.	MgO-C blend and C in the absence of MgO.	MgO-C blends.
Method	<ol style="list-style-type: none"> Set the fraction of O₂ in the sweep. Set the flow rate of the O₂-Ar sweep. Set the initial amount of C to $N_{\text{ClO}_2}^0$. Set the initial amount of MgO to N_{MgO}^0. Blend $N_{\text{ClO}_2}^0$ with N_{MgO}^0. Subject the MgO-C blend prepared in step 5 to the standard temperature program. Determine the temporal amounts of CO in the product gas and the extent of CTR. Subject $N_{\text{ClO}_2}^0$ alone to the standard temperature program but in the absence of MgO. Determine the temporal amounts of CO in the product gas. Compare the temporal amounts of CO in the product gas acquired in steps 7 and 9. Locate the onset of CTR ($\tau_1 _{\text{O}_2}$) as the moment at which the temporal amounts of CO acquired in steps 7 and 9 start deviating from each other. Determine $\tilde{N}_{\text{ClO}_2}(\tau_1)$, $\tilde{N}_{\text{ClO}_2}(\tau_f)$ and the partial pressure of CO ($\tilde{p}'_{\text{CO} _{\text{O}_2}}$) from the test exploiting C in the absence of MgO (step 8). 	<ol style="list-style-type: none"> Set the initial fraction of CO₂ in the sweep. Set the initial flow rate of the CO₂-Ar sweep. Set the initial amount of C to $N_{\text{ClCO}_2}^0$. Set the initial amount of MgO to N_{MgO}^0 (the same value used in step 4 of phase 1). Blend $N_{\text{ClCO}_2}^0$ with N_{MgO}^0. Subject the MgO-C blend prepared in step 5 to the standard temperature program. Determine temporal amounts of CO in the product gas. Subject $N_{\text{ClCO}_2}^0$ alone to the standard temperature program but in the absence of MgO. Determine temporal amounts of CO in the product gas. Compare the temporal amounts of CO in the product gas acquired in steps 7 and 9. Locate the onset of CTR ($\tau_1 _{\text{CO}_2}$) as the moment at which the temporal amounts of CO acquired in steps 7 and 9 start deviating from each other. Determine $\tilde{N}_{\text{ClCO}_2}(\tau_1)$ and $\tilde{N}_{\text{ClCO}_2}(\tau_f)$ from the test exploiting C in the absence of MgO (step 8). Check if $\tilde{N}_{\text{ClO}_2}(\tau_1) \approx \tilde{N}_{\text{ClCO}_2}(\tau_1)$ and $\tilde{N}_{\text{ClO}_2}(\tau_f) \approx \tilde{N}_{\text{ClCO}_2}(\tau_f)$. If not, go back to steps 1-3 and vary the CO₂ fraction, and/or the sweep flow rate, and/or $N_{\text{ClCO}_2}^0$. For the initial amount of C, the CO₂ fraction in the sweep, and the flowrate of the CO₂-Ar sweep identified at steps 1-3, determine the partial pressure of CO ($\tilde{p}'_{\text{CO} _{\text{CO}_2}}$). Blend N_{MgO}^0 with the $N_{\text{ClCO}_2}^0$ identified in step 3. Subject the MgO-C blend prepared in step 15 to the standard temperature program under the CO₂-Ar sweep gas mixture flow rate and CO₂ fraction identified at steps 1 and 2. Determine the extent of CTR. 	<ol style="list-style-type: none"> Prepare two pairs of MgO-C blends, each by mixing the initial amount of MgO selected in phase 1 with the initial amounts of C $\tilde{N}_{\text{C}}(\tau_1)$ and $\tilde{N}_{\text{C}}(\tau_f)$ identified in Phase 1. Subject each of the prepared blends to the same temperature program under the Ar sweep and the CO-Ar sweep having the CO partial pressure equal to $\tilde{p}'_{\text{CO} _{\text{CO}_2}}$ observed in step 14 of phase 2.

S3 Weight fractions of impurities in the starting materials

The weight fractions of H₂O and CO₂ in the as-received MgO ($w_{\text{MgO}}^{\text{imp}}$) and in the as-received Al₂O₃ ($w_{\text{Al}_2\text{O}_3}^{\text{imp}}$) were determined by thermogravimetry (Netzsch 409 STA). Samples of as-received materials were heated in Ar up to 1000°C at a rate of 20°C/min and held at this temperature for one hour. The measured mass loss corresponded to the total mass of adsorbed and chemisorbed H₂O and CO₂ in the as-received materials.

The as-received charcoal contained moisture, volatile matter, and ash. To determine their weight fractions, a sample of as-received charcoal was placed into a thermogravimetric analyzer (Netzsch 409 STA), heated to 105°C in Ar at a rate of 20 °C/min, and then kept at this temperature for 30 minutes. The measured mass loss corresponded to the mass of moisture contained in the as-received material. Then, the temperature was increased to 1000°C at a rate of 20 °C/min and then maintained constant for 30 minutes to determine the mass loss due to evaporation of the volatile matter. The atmosphere was then switched to a 20% Ar-air and kept until the sample mass stabilized indicating the mass of ash after the complete oxidation of C.

S4 Determination of the mass of the unreacted MgO in the residual reactant blend

The recovered residual reactant blend was first weighed to determine its mass (m^f) and then stirred well in a pill glass with a spatula. In the next step, a sample of the homogenized blend amounting to m_s^0 was heated under a 20% air/Ar atmosphere at a rate of 20°C/min to 900°C. The sample was held at this temperature until its mass stabilized at m_s^f , indicating that all the remaining C was oxidized thus leaving the retainer comprising only MgO and ash. The mass of the unreacted MgO in the residual reactant blend m_{MgO}^f was then calculated as

$$m_{\text{MgO}}^f = m_s^f - \frac{m_s^0}{m^f} w_{\text{ash}}^C \underbrace{(m_2^0 + m_C^*)}_{m_{\text{ash}}^0}. \quad (\text{S3})$$

S5 Outlet molar rates of product gases

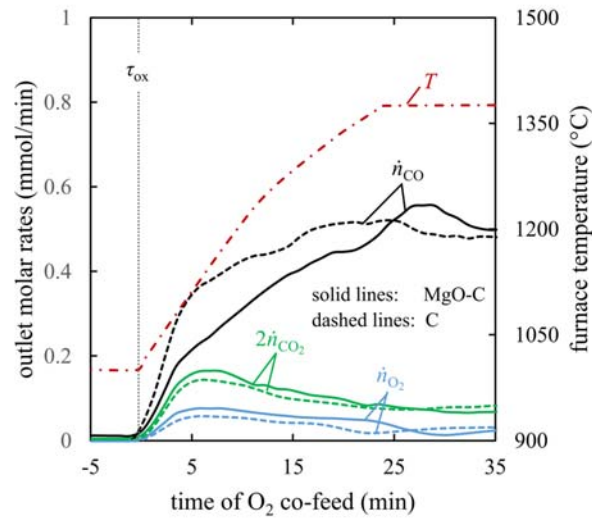


Figure S2. Outlet molar rates of CO, CO₂, and O₂ for MgO-C and C alone subjected to the O₂-Ar sweep at $T_{SP}=1375^{\circ}\text{C}$. Note: the mole rate of CO₂ is shown doubled to ease visual distinction from the mole rate of O₂.

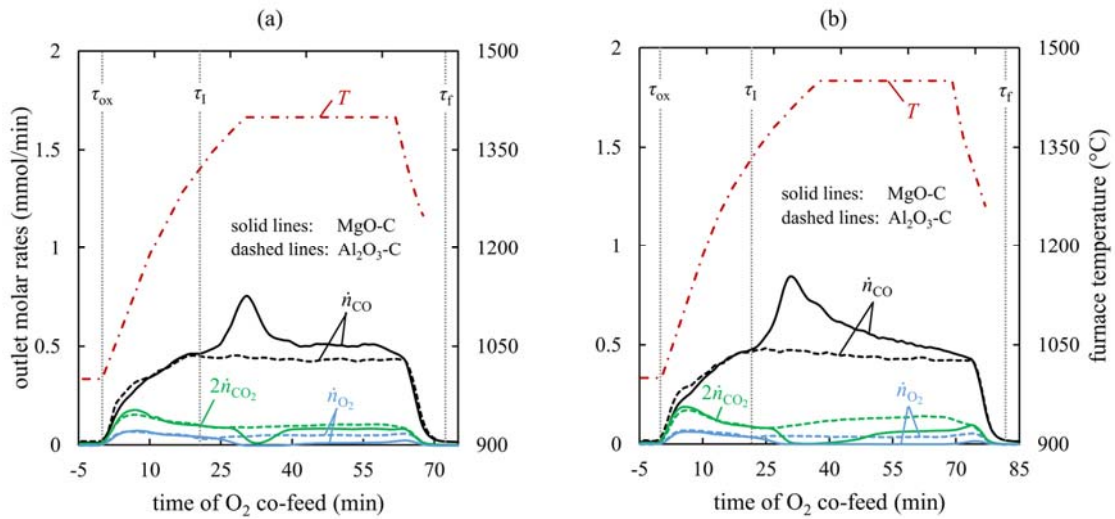


Figure S3. Outlet molar rates of CO, CO₂, and O₂ for MgO-C and Al₂O₃-C blends subjected to the O₂-Ar sweep at (a) $T_{SP}=1400^{\circ}\text{C}$ and (b) $T_{SP}=1450^{\circ}\text{C}$. Note: the mole rate of CO₂ is shown doubled to ease visual distinction from the mole rate of O₂.

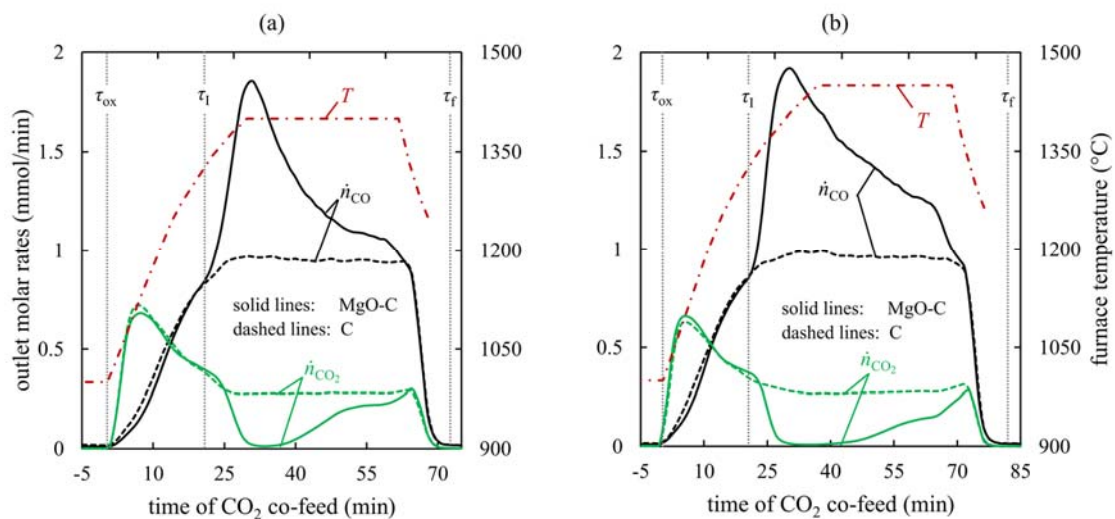


Figure S4. Outlet molar rates of CO and CO₂ for MgO-C and C alone subjected to the CO₂-Ar sweep at (a) $T_{SP} = 1400^\circ\text{C}$ and (b) $T_{SP} = 1450^\circ\text{C}$.

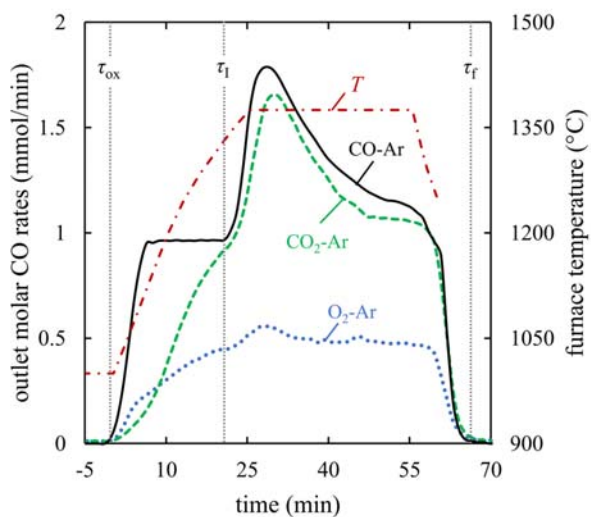


Figure S5. CO molar rates observed at $T_{SP} = 1375^\circ\text{C}$ with $N_C^0|_{high} \approx \tilde{N}_C(\tau_1) = 47.5$ mmol and $N_{MgO}^0 = 49.6$ mmol under CO-Ar (black solid line), CO₂-Ar (green dashed line) and O₂-Ar (blue dotted line).

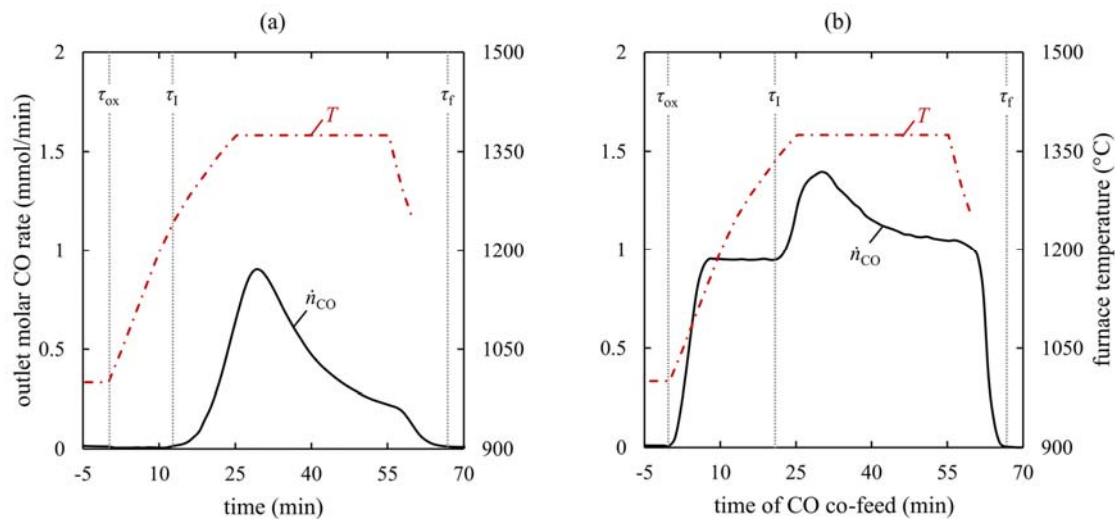


Figure S6. Outlet molar rates of CO at $T_{SP} = 1375^\circ\text{C}$ for (a) Ar alone with $N_C^0|_{high} \approx \tilde{N}_C(\tau_1) = 47.5$ mmol and (b) CO-Ar sweep with $N_C^0|_{low} \approx \tilde{N}_C(\tau_f) = 32.9$ mmol.

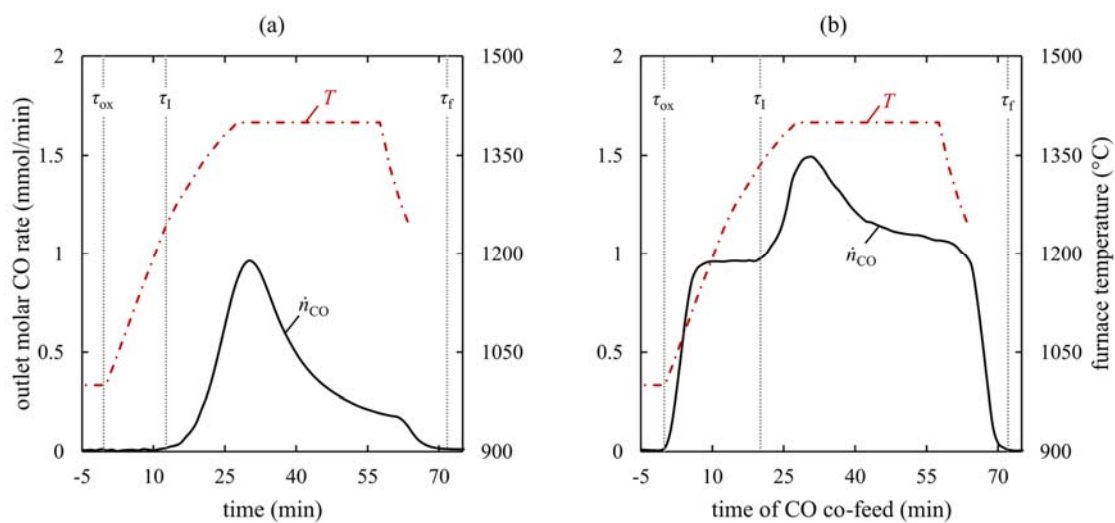


Figure S7. Outlet molar rates of CO at $T_{SP} = 1400^\circ\text{C}$ for (a) Ar alone with $N_C^0|_{high} \approx \tilde{N}_C(\tau_1) = 47.5$ mmol and (b) CO-Ar sweep with $N_C^0|_{low} \approx \tilde{N}_C(\tau_f) = 31.6$ mmol.

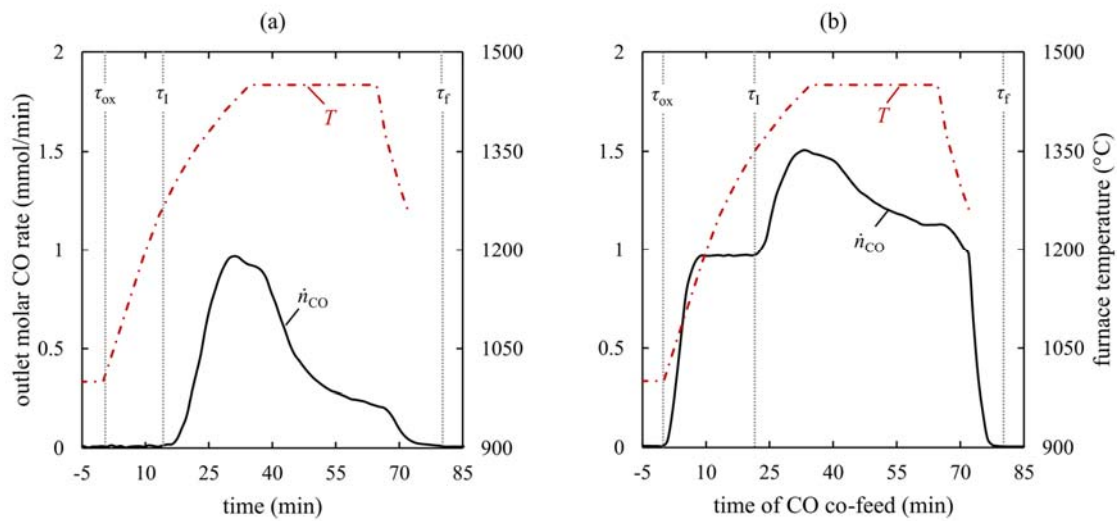


Figure S8. Outlet molar rates of CO at $T_{SP} = 1450^\circ\text{C}$ for (a) Ar alone with $N_C^0|_{high} \approx \tilde{N}_C(\tau_1) = 47.5$ mmol and (b) CO-Ar sweep with $N_C^0|_{low} \approx \tilde{N}_C(\tau_f) = 26.6$ mmol.

S6 Repeatability of the experimental setup

The repeatability of the experimental setup was inspected by reacting two MgO-C blends prepared in the same way as described in section 3.4 under the same experimental conditions. The results are shown in Figure S9.

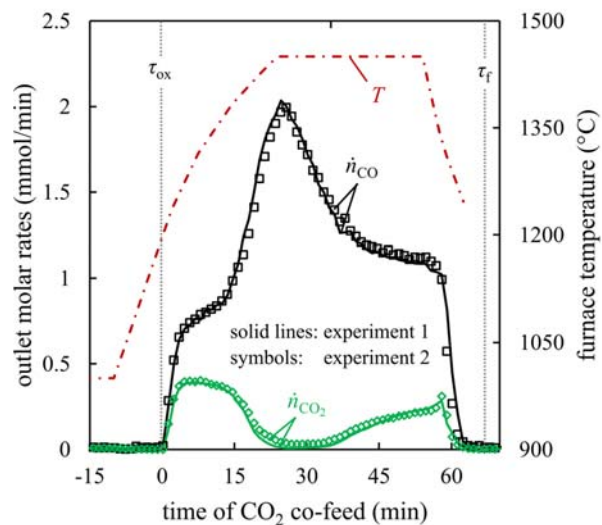


Figure S9. Outlet CO and CO₂ molar rates from two replicate experiments under a 5% CO₂-Ar sweep at $T_{SP} = 1450^{\circ}\text{C}$: $N_{\text{MgO}}^0 = 49.6$ mmol (Sigma-Aldrich, # 342793), $N_{\text{C}}^0 = 53.3$ mmol (Fluka Analytical #05105), the total flow rate of the CO₂-Ar sweep (0.4 L_N/min). The CO₂-Ar sweep commenced to the setup at 1200°C.

S7 Comparison of the amounts of C and partial pressures of CO in the absence of MgO

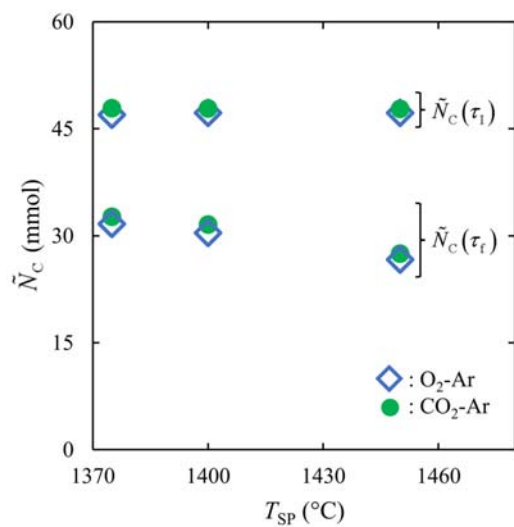


Figure S10. Comparison of $\tilde{N}_c(\tau_1)$ and $\tilde{N}_c(\tau_f)$ under the O₂-Ar and the CO₂-Ar sweeps as function of T_{SP} .

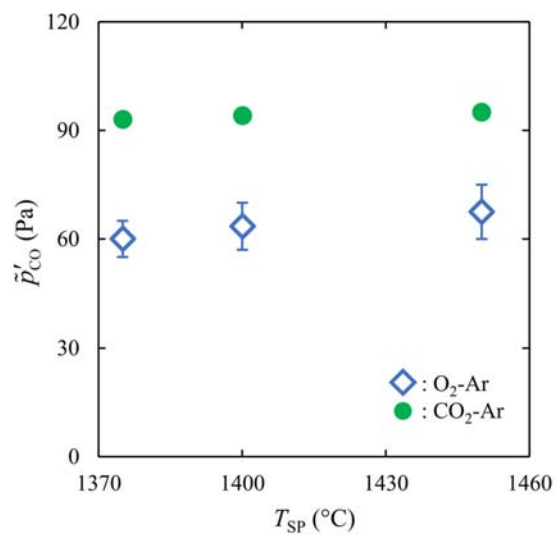


Figure S11. Partial pressures of CO ($\tilde{p}'_{CO}|_{O_2}$ and $\tilde{p}'_{CO}|_{CO_2}$) at T_{SP} in the absence of CTR.

S8 Effect of atmosphere on MgO sintering

The effect of atmosphere on MgO sintering was evaluated by subjecting samples of the as-received MgO powder (Sigma Aldrich, no. 342793, see Table 1 in section 3.2) to the temperature program illustrated in Figure S12 (Netzsch 409 STA thermogravimeter) as follows. First, the sample was heated under 0.1 L_N/min N₂ (Messer 4.7) with a rate of 20°C/min to a desired temperature T_{sint} ranging from 900-1200°C and kept there for 5 min to ensure the complete dissociation of the Mg(OH)₂ and MgCO₃ impurities from the samples. The samples were then sintered for additional 15 min under 0.1 L_N/min of N₂ (Messer 4.7), 20.5% O₂-N₂ (synthetic air, Messer) or 20.5% CO₂-N₂ (obtained by mixing N₂ (Messer 5.0) with CO₂ (Messer 4.8)). Upon the completion of the sintering step, the samples were cooled at a rate of 20°C/min. The SSA's of the samples were analyzed using the BET method (Micrometrics TriStar 3000 N₂ adsorption analyzer) in Figure S13. While this figure does indicate a significant decrease from the SSA of the as-received MgO (141 m²/g) with an increase in the sintering temperature, the sintering atmosphere does not seem to have an effect.

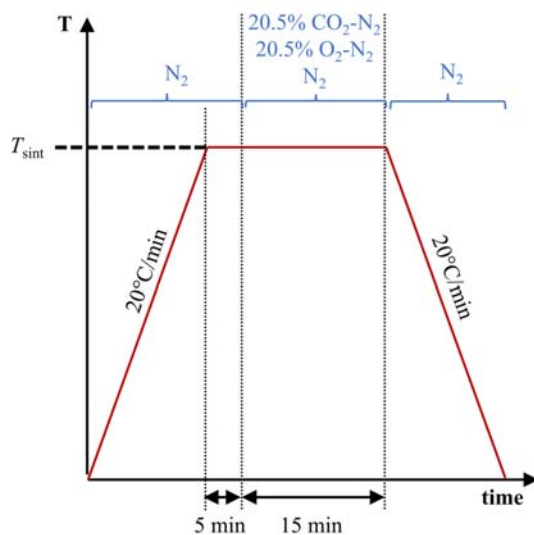


Figure S12. MgO sintering conditions.

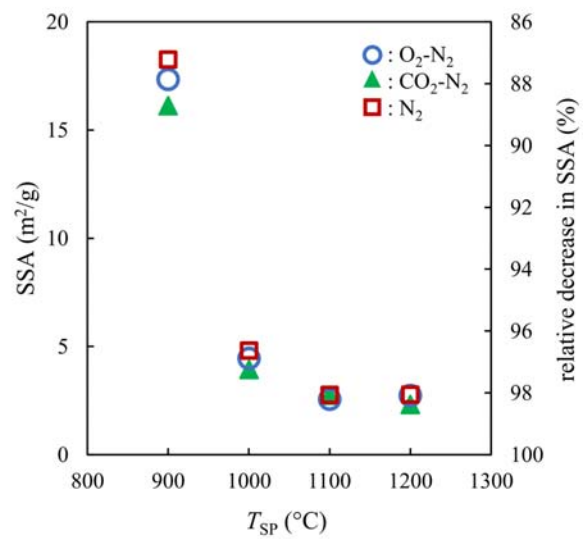


Figure S13. Effect of O₂ and CO₂ on MgO surface area during sintering.

S9 Assessment of the average effective partial pressures of Mg in the hot zone based on the experimentally observed Mg productions

The average partial pressures of Mg in the hot zone during the comparison runs under the O₂-Ar and CO₂-Ar sweeps ($\bar{p}'_{\text{Mg}}|_{\text{int}}$) were assessed based on the average production rate of Mg by the CTR ($\bar{n}'_{\text{Mg}}|_{\text{int}}$) calculated as

$$\bar{n}'_{\text{Mg}}|_{\text{int}} = \left[\frac{\xi_1(\tau_f)}{\tau_{\text{II}} - \tau_1} \right]_{\text{int}} \quad (\text{S4})$$

where $\xi_1(\tau_f)|_{\text{int}}$ is the extent of the CTR and $(\tau_{\text{II}} - \tau_1)|_{\text{int}}$ is the total reduction time. Because of the high dilution of the product gas with Ar ($y_{\text{Ar}}(t) \approx 0.9-0.95$), the total molar rate did not change significantly between the hot zone and the outlet, i.e.

$$\dot{n}(t) \approx \dot{n}'(t) \quad (\text{S5})$$

which allowed calculating the average partial pressure of Mg in the hot zone as

$$\bar{p}'_{\text{Mg}}|_{\text{int}} = \left[\frac{\bar{n}'_{\text{Mg}}}{\bar{n}} \bar{p}_{\text{tot}} \right]_{\text{int}} \quad (\text{S6})$$

As the extents of CTR were only approximated within the uncertainty range bound by the maximum possible amount of deposited C (see equations 30 and 35), the corresponding ranges for $\bar{p}'_{\text{Mg}}|_{\text{int}}$ are listed in Table S2.

Table S2. Uncertainty ranges of the average partial pressures of Mg in the hot zone under the O₂-Ar and CO₂-Ar sweep.

T_{SP} (°C)	$\bar{p}'_{\text{Mg}} _{\text{O}_2}$ (Pa)	$\bar{p}'_{\text{Mg}} _{\text{CO}_2}$ (Pa)
1375	10-16	25-31
1400	12-19	27-34
1450	16-22	28-35

S10 Assessment of the partial pressures of Mg in the hot zone expected from the equilibrium of reactions 2 and 4

S10.1 O₂-Ar sweep

The high limit of the equilibrium partial pressures of Mg in the hot zone resulting from reaction 2

$$p'_{\text{Mg,eq}}|_{\text{O}_2} = \left[\frac{K_2(T)}{(p'_{\text{O}_2})^{0.5}} \right]_{\text{O}_2} \quad (\text{S7})$$

can be estimated under the O₂–Ar sweep using the outlet molar rates of O₂ shown in Figure 4 and Figure S3 considering that these rates could only be lower than the O₂ molar rates in the hot zone because of the potential additional consumption of O₂ in the cooling zone via reactions 6 and 7. Therefore, as the outlet O₂ molar rates can be considered as a lower limit of the O₂ molar rates in the hot zone, i.e. $\dot{n}_{\text{O}_2}(t)|_{\text{O}_2} \leq \dot{n}'_{\text{O}_2}(t)|_{\text{O}_2}$, and invoking equation S5 one may bound the O₂ partial pressure in the hot zone as

$$p'_{\text{O}_2}(t)|_{\text{O}_2} \geq \left[\frac{\dot{n}_{\text{O}_2}(t)}{\dot{n}(t)} p_{\text{tot}}(t) \right]_{\text{O}_2} \quad (\text{S8})$$

The results of the calculations via equations S7 and S8 are shown in Table S3. One should note that no result could be reported for $T_{\text{sp}} = 1450^\circ\text{C}$, as the partial pressure of O₂ may have been zero for a part of the experiment.

Table S3. Low limits of the O₂ molar rates in the hot zone and the corresponding high limits of the equilibrium partial pressures of Mg of reaction 2 in the hot zone under the O₂-Ar sweep.

T_{sp} (°C)	$p'_{\text{O}_2} _{\text{O}_2}$ (Pa)	$p'_{\text{Mg,eq}} _{\text{O}_2}$ (Pa)
1375	1.7	$9 \cdot 10^{-6}$
1400	0.2	$5.4 \cdot 10^{-5}$
1450	0	(-)

S10.2 CO₂-Ar sweep

Under the CO₂-Ar sweep, the equilibrium partial pressures of Mg_(g) ($p'_{\text{Mg,eq}}|_{\text{CO}_2}$) resulting from reaction 4 may be estimated based on equation S2 of section S1 of ESI that was reformulated as

$$p'_{\text{Mg,eq}}|_{\text{CO}_2} = K_4(T) \left[\frac{p'_{\text{CO}}}{p'_{\text{CO}_2}} \right]_{\text{CO}_2} \quad (\text{S9})$$

However, the additional consumption of both CO and CO₂ in the cooling zone via reverse reactions 1 and 4 precludes the direct determination of the $p'_{\text{CO}}|_{\text{CO}_2}$ and the $p'_{\text{CO}_2}|_{\text{CO}_2}$ based on the outlet molar rates. These partial pressures could still be estimated as follows.

- Compared to the outlet molar CO rate ($\dot{n}_{\text{CO}}(t)|_{\text{CO}_2}$), the molar rate of CO in the hot zone ($\dot{n}'_{\text{CO}}(t)|_{\text{CO}_2}$) may have been either (i) higher due to the consumption of CO in the cooling zone by the reverse reaction 1 depositing C, or (ii) lower due to the production of CO via reverse reaction 4 proceeding either in the hot and/or cooling zone. The molar rates of CO in the hot zone were the highest under the assumption that reverse reaction 4 proceeded in the hot zone only. In this case, the material balance of CO between hot zone and outlet is given as

$$\dot{n}_{\text{CO}}(t)|_{\text{CO}_2} = \left[\dot{n}'_{\text{CO}}(t) - \dot{n}_{\text{C,dep}}(t) \right]_{\text{CO}_2} \quad (\text{S10})$$

with $\dot{n}_{\text{C,dep}}(t)|_{\text{CO}_2}$ as the deposition rate of C (i.e. the consumption rate of CO) in the cooling zone. Assuming that $\dot{n}_{\text{C,dep}}(t)|_{\text{CO}_2}$ scales proportionally with $\dot{n}'_{\text{CO}}(t)|_{\text{CO}_2}$, i.e. the reaction order of the reverse reaction 1 is unitary with respect to CO, $\dot{n}_{\text{C,dep}}(t)|_{\text{CO}_2}$ can be written as

$$\dot{n}_{\text{C,dep}}(t)|_{\text{CO}_2} = \left[Z \cdot \dot{n}'_{\text{CO}}(t) \right]_{\text{CO}_2}, \quad (\text{S11})$$

with Z as the fraction of $\dot{n}'_{\text{CO}}(t)|_{\text{CO}_2}$ consumed that is constant with time. Solving equation S11 for $\dot{n}'_{\text{CO}}(t)|_{\text{CO}_2}$ and combining with equation S10 yields

$$\dot{n}_{\text{CO}}(t)|_{\text{CO}_2} = \left[\dot{n}_{\text{C,dep}}(t) \left(\frac{1}{Z} - 1 \right) \right]_{\text{CO}_2} \quad (\text{S12})$$

By integrating equation S12 over the total time of the CTR ($\tau_{\text{II}} - \tau_1$), and considering that

$$\left[N_{\text{C,dep}}(\tau_{\text{II}}) - N_{\text{C,dep}}(\tau_1) \right]_{\text{CO}_2} = N_{\text{C,dep}}(\tau_f)|_{\text{CO}_2}, \quad (\text{S13})$$

allows evaluating the fraction Z as

$$Z = \left[\frac{N_{\text{C,dep}}(\tau_f)}{N_{\text{CO}}(\tau_{\text{II}}) - N_{\text{CO}}(\tau_1) + N_{\text{C,dep}}(\tau_f)} \right]_{\text{CO}_2} \quad (\text{S14})$$

The molar rate of CO in the hot zone can be estimated by combining equations S10 and S11

$$\dot{n}'_{\text{CO}}(t)|_{\text{CO}_2} = \left[\left(\frac{1}{1-Z} \right) \dot{n}_{\text{CO}}(t) \right] |_{\text{CO}_2} \quad (\text{S15})$$

resulting in the values shown in Table S4.

- The molar rate of CO₂ in the hot zone $\dot{n}'_{\text{CO}_2}(t)|_{\text{CO}_2}$ could have only been higher than the outlet CO₂ molar rates $\dot{n}_{\text{CO}_2}(t)|_{\text{CO}_2}$ because reverse reaction 4 consumes CO₂. Thus, the low limit of $\dot{n}'_{\text{CO}_2}(t)|_{\text{CO}_2}$ are given as (see Table S4)

$$\dot{n}'_{\text{CO}_2}(t)|_{\text{CO}_2} \geq \dot{n}_{\text{CO}_2}(t)|_{\text{CO}_2} \cdot \quad (\text{S16})$$

With $p'_{\text{CO}}/p'_{\text{CO}_2} = \dot{n}'_{\text{CO}}/\dot{n}'_{\text{CO}_2}$, the values of $p'_{\text{Mg,eq}}|_{\text{CO}_2}$ calculated via equation S9 are listed in Table S4.

Table S4. Fractions of CO spent on the depositing C in the cooling zone, high limits of molar CO rates in the hot zone, low limits of molar CO₂ rates in the hot zone, and corresponding high limits of the reaction (4) equilibrium partial pressures of Mg_(g) expected in the hot zone under the CO₂-Ar sweep.

T_{SP} (°C)	Z (-)	$\dot{n}'_{\text{CO}} _{\text{CO}_2}$ (mmol/min)	$\dot{n}'_{\text{CO}_2} _{\text{CO}_2}$ (mmol/min)	$p'_{\text{Mg,eq}} _{\text{CO}_2}$ (Pa)
1375	0.041	1.7	0.023	0.07
1400	0.042	1.9	0.013	0.24
1450	0.045	2.0	0.007	1.18

S11 Normalized extents of the CTR

Table S5. Normalized extents of the CTR presented in Figure 7.

data set #	(I)	(II)	(III)	(IV)	(V)
sweep	Ar	CO-Ar	CO ₂ -Ar	CO-Ar	O ₂ -Ar
T_{SP} (°C)					
1375	0.310	0.275	0.165-0.205	0.160	0.070-0.110
1400	0.350	0.295	0.195-0.245	0.185	0.090-0.140
1450	0.400	0.375	0.260-0.320	0.220	0.150-0.210

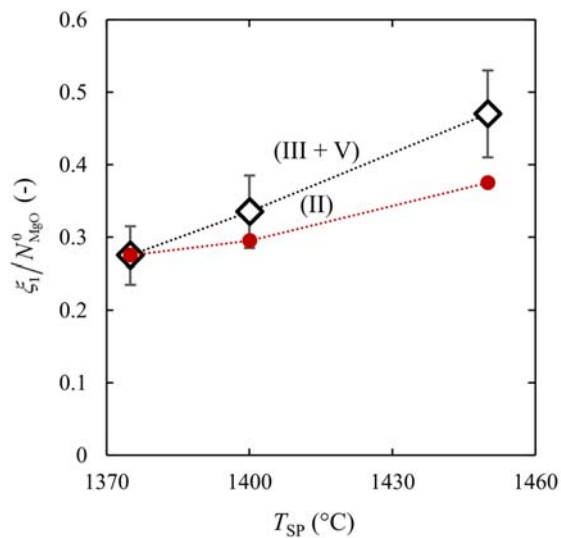


Figure S14. Sum of the normalized extents of the CTR under the CO₂-Ar and the O₂-Ar sweeps (data sets III and V from Figure 7) in comparison to the normalized extents of the CTR under the CO-Ar sweep (data set II from Figure 7).

Bibliography

1. A. Roine, Outokumpu HSC Chemistry for Windows 5.0, Outokumpu Research Oy, Finland, 2002